Adsorption and Aggregation at Silica/Methanol Interfaces: The Role of Solute Structure

*B. Lauren Woods, Jenna K. George, Alex M. Sherman, Patrik R. Callis, and Robert A. Walker**

Department of Chemistry and Biochemistry, Montana State University, Bozeman MT 59717

Supporting Information

Computational data from different DFT Functionals.

Additional geometry optimization calculations were performed using CAM-B3Lyp, a range separated, hybrid functional. Although CAM-B3Lyp was designed for calculating long range interactions, the M06L method proved to have consistently lower (or more negative) energies, as shown in Table S1. The 2x the monomer optimized energy was subtracted from the dimer energies to determine the stabilization resulting from dimer formation, ΔE_{dimer}. A large magnitude difference would imply C152 prefers to form dimers in lieu of have single monomers. The table includes the ΔE_{dimer} calculated using both the M06L and CAM-B3Lyp methods, the energetics are given both in units of kJ/mol and a.u. Additionally, many unfavorable starting positions resulted in an optimized geometry that was markedly different from the initial arrangement. In Table B.1 if the final geometry was different than the starting geometry, the energy recorded is the optimized energy of the initial geometry. Additionally, many unfavorable starting positions resulted in an optimized geometry that was markedly different from the initial

arrangement. In Table S1 if the final geometry was different than the starting geometry, an * was added either to the row or to individual values.

Table S.1: Calculated energetics of dimers formation with various starting orientations in two different units.

	CAM-B3lyp			M06L		
Orientation	Vac (kJ/mol) (au)	Hex (kJ/mol) (au)	MeOH (kJ/mol) (au)	Vac (kJ/mol) (au)	Hex (kJ/mol) (au)	MeOH (kJ/mol) (au)
SS anti	-23.8120 -0.0091	-16.9597 -0.0065	-6.4297 -0.0025	-33.3696 0.0109	-26.5460 -0.0188	-15.2681 -0.0208
SS para*	86.8137 0.0331	88.0622 0.0336	89.2133 0.0340	65.3521 0.0485	-4.2805 0.0000	-3.8292 -0.0164
Stacked anti	-23.8120 -0.0091	-17.6623 -0.0067	-6.4297 -0.0025	-74.8892 -0.0285	-68.1592 -0.0260	-57.8589 -0.0220
Stacked para*	815.9805 0.3109	88.0622 0.0331	817.7958 0.3116	734.7998 0.3036	-4.2805 0.0485	298.7609 0.0989
Head to tail	--- ---	--- ---	--- ---	107.6818 0.0647	110.5058 0.0334	116.9673 0.0296

To estimate the effect of aggregation of C152 on the surface, we have examined the computed, frequency dependent hyperpolarizability (β) values in the output from Gaussian 09 calculations for monomer and dimer forms of C152 with input route cards of the form:

 # method/basis polar=dcshg nosym pop=reg

The region of resonance was determined from corresponding calculations with the route card:

 # method/basis td(nstates=N) nosym pop=reg

where N is an integer in the range 3-10 as required to capture the energy of the lowest strongly absorbing excited state.

The β term represents the likelihood of inducing a dipole in a molecule and is related to the second order susceptibility $\chi^{(2)}$ through Equation 3 in the main text. Although β is a combination of hyperpolarizabilities, experimentally SHG can only detect contributions from 4 unique terms, β_{zzz}, $\beta_{izi,}$, β_{iiz}, and β_{zii}, where the dipole is aligned parallel to β_{zzz}. Computationally, the strongest response came from our assigned β_{zzz}, as expected. The calculations were performed under ideal conditions, where the dimers were overlapped almost completely. Table S.2 shows the calculated resonance wavelength and β_{zzz} for monomer and dimer formation of C152 in vacuum, methanol, and n-hexane. The ratio of the monomer to dimer was also calculated and for direct comparison, the β_{zzz} of the monomer was doubled. The data shows almost a 14-fold decrease in hyperpolarizability values going from a monomer to dimer formation. As the second harmonic response is proportionally to β^2, the computational data suggests that in ideal conditions, the second harmonic signal should see about a 200-fold decrease in signal in nonpolar environments. In a polar continuum, dimerization resulted in only about a 40-fold decrease in signal. The computational data supports the hypothesis that the dimers are oriented in such a way to form an inversion center which would result in a decrease in SHG response. Experimental methods do not provide the sensitivity to distinguish between individual dimer formations and orientation, computational results can provide insight into the likely dipole-dipole interactions. As the SHG signal did not show a 200-fold decrease in signal, the dipole moments appears not to be overlapped completely.

Table S.2: Calculated hyperpolarizability of monomers and of dimers in vacuum, methanol, and n-hexane.

	Vacuum		Methanol		n-Hexane	
	Monomer	Dimer	Monomer	Dimer	Monomer	Dimer
λres (nm)	785.0	812.9	865.0	868.5	827.0	845.7
$\beta_{(zzz)}$ (au)	4.61E+06	-3.36E+05	3.60E+06	-5.85E+05	8.15E+06	-6.39E+05
Ratio ($\beta_{2xmono}/\beta_{dimer}$)	13.7		6.2		12.8	

Second Harmonic Generation (SHG) was used to collect spectra of C152 at the methanol/silica interface at three different concentrations. The three concentrations were chosen based on the isotherm spectrum shown in Figure S.1A, the normalized spectra are shown in Figure S.1B. The concentrations were chosen before monolayer coverage (30 μM), at monolayer coverage (80 μM), and after aggregation (300 μM). As evident from Figure S.1, all three spectra overlaps and there are no discernible differences in line shape. The data suggest that the C152 being sampled in the SHG experiments is experiencing the same solvation environment throughout the aggregation process.

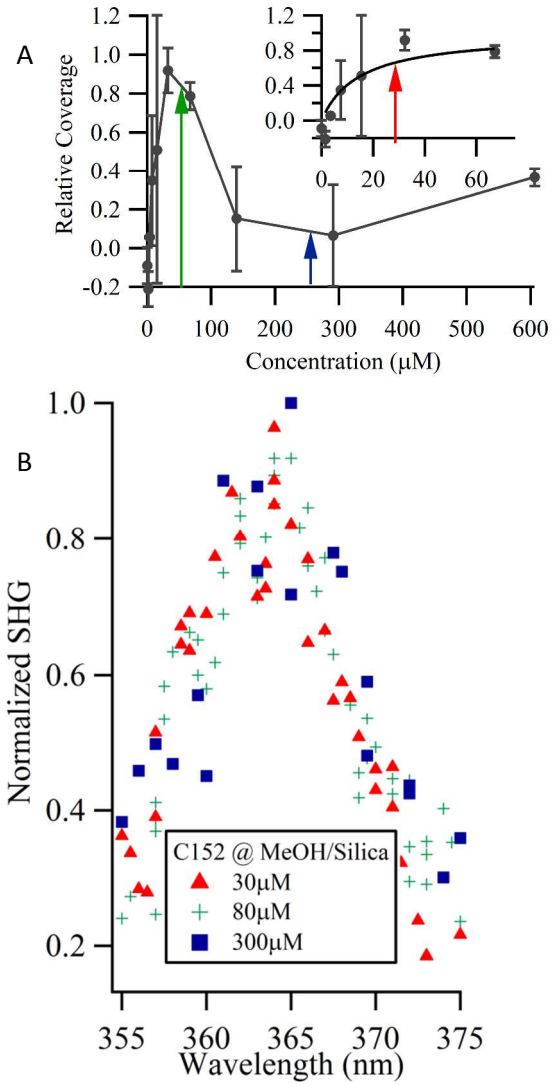

Figure S.1: SHG spectra of C152 at the MeOH/silica interface at 3 concentrations.

Time resolved fluorescence at different wavelengths.

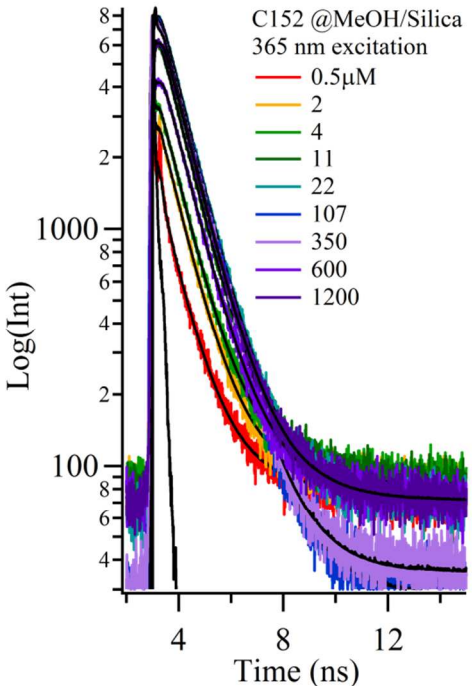

Figure S.2: Time resolved decays for C152 at MeOH/silica interface with an excitation of 365nm and collected at 513nm. The IRF is shown in black.

Time resolved fluorescence data were collected at total internal reflection geometry using the excitation wavelength of 365 nm, the resonance wavelength calculated from SHG data. No filters were added for the decays found in Figure S.2. Fitting the decays to two lifetimes yielded values of ~0.9 ns and ~2 ns at lower concentrations, however as concentration increased the lifetime assigned to the interfacial behavior, ~3 ns, had diminishing contribution. At concentrations where aggregation is occurring, the decays did not show any distinguishing changes. As reported in the manuscript, when exciting C152 adsorbates at 396 nm, at concentrations >300 μM a second longer lifetime was visible. The lower excitation wavelength did not appear to excite the aggregates efficiently.

Additional decays were taken following excitation at 396 nm using the TIR geometry for a large range of concentrations. Figure S.3 shows the decays taken when monitoring emission at 574 nm, the emission peak assigned to aggregation at the solid/vapor interface. Data on the left were acquired using a 420 nm long pass filter and data on the right resulted from further filtering the emission using a 530 nm long pass filter. These filters allow for separation of the aggregation peak and the bulk emission peak, at 513 nm. The decays collect at 513 nm were shown in the

manuscript, but in comparison, the addition of filters did not alter the values of the lifetimes but did make drastic differences in relative contributions, as discussed in the manuscript.

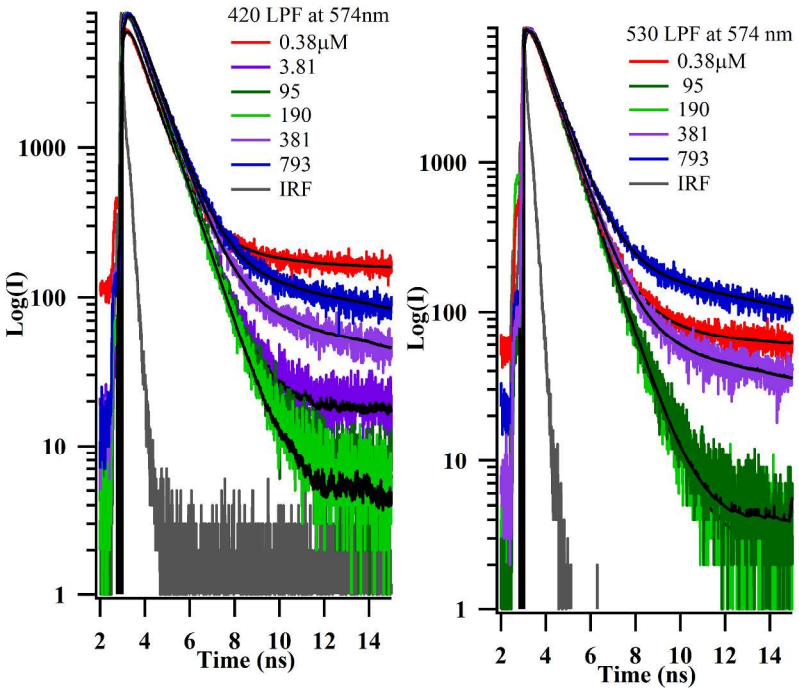

Figure B.3: Time resolved decays for C152 at MeOH/silica interface exciting at 396 nm and collected at 574 nm using two different long pass filters. Fits are shown in black.